Picosecond photoexcitation of acoustic waves in locally canted gold films

T. Pezeril,[1,2,a)] F. Leon,[3] D. Chateigner,[3] S. Kooi,[2] and Keith A. Nelson[2]
[1]*Laboratoire de Physique de l'Etat Condensé, UMR CNRS 6024, Université du Maine, 72000 Le Mans, France*
[2]*Department of Chemistry, Massachusetts Institute of Technology, Cambridge, Massachusetts 02139, USA*
[3]*Crismat-Ensicaen, UMR CNRS 6508, Université de Caen Basse-Normandie, 14050 Caen, France*

(Received 13 November 2007; accepted 21 January 2008; published online 13 February 2008)

The laser photoacoustic technique is used to generate and detect picosecond coherent acoustic vibrations in gold film media deposited on Si substrates. As a consequence of the gold crystallites' canted orientation, the pump-probe picosecond transient reflectivity shows oscillations at the fundamental shear mode frequency. The shear character of the mode is suggested by its dispersion, by the dependence of the signal on the probe laser wavelength, and by x-ray texture analysis.
 [DOI: 10.1063/1.2841823]

The development of picosecond ultrasonics,[1–3] in which single-cycle acoustic wavepackets are generated through sudden laser heating of a thin film and are detected optically after propagation through one or more film and/or substrate layers, has been exploited for thin film diagnostics and for measurement of acoustic properties in the ~50–500 GHz frequency and ~10–100 nm wavelength ranges. The method has been applied to a wide range of materials, but in general it has been restricted to generation and characterization of longitudinal acoustic waves.[4] High-frequency, short-wavelength shear acoustic properties would be of great interest in many materials, especially disordered and partially ordered systems such as supercooled liquids and glasses, mixed ferroelectrics and multiferroics, and giant magnetoresistance or other correlated electron systems in which fast relaxation dynamics or mesoscopic correlation lengths of quantities that are coupled to shear play important roles. Recently, examples have emerged in which the transverse isotropic symmetry of the sample structure is broken in order to permit shear wave generation through sudden laser heating. Thus, shear acoustic wave components were generated in an off-axis oriented Zn single crystal[4–7] or by use of an off-axis TeO_2 transparent substrate coated by an Al layer.[8] These examples illustrated possibilities for shear wave generation, but their requirements for specialized material fabrication or acoustic wave generation conditions reduce their versatility for use with a wide range of materials. In the present letter, we demonstrate shear wave generation and detection in an extremely simple system: a thin gold film on a silicon single crystal substrate. We describe experimental observation of a fundamental shear mode of vibration in addition to the fundamental longitudinal mode observed ordinarily.[1–3,9–14] X-ray texture analysis shows that shear wave generation results from the distribution of nanocrystallite orientations in a gold layer that is fabricated through routine dc sputtering.

The samples are thin gold films of different thicknesses deposited on silicon (100) single crystals by dc sputtering. The current during deposition was set at 10 mA, pressure before deposition was 6×10^{-2} mbar, argon pressure during deposition around 10^{-1} mbar, and the gold target was at a distance of about 7 cm from the substrate at room temperature. The thicknesses of the films were measured using x-ray reflectivity,[15] with an accuracy of ~0.1 nm. X-ray combined analysis[16] has been used to quantitatively determine the crystallographic textures, mean crystallite sizes, and cell parameters of the gold films. The full x-ray diagrams were collected on a four-circle diffractometer in order to extract gold pole figures. These were used as crystallographic texture inputs in order to refine the orientation distribution function[17] (ODF) of the crystallites in the films, refined within reliability factors of around 3%.[18–20] The pole figures recalculated from the ODF are expressed in multiples of a random distribution unit (m.r.d.), 1 m.r.d. being the value for a randomly oriented sample. They are represented here as radial density functions since all the textures we observed were axially symmetric about the sample normals. The ODF was then used to calculate the macroscopic elastic stiffness tensors of the films starting from the tensor of the single crystal weighted using the geometric mean approach.[21] The macroscopic stiffness tensor obtained yielded longitudinal and transverse acoustic velocities along the sample's normals of 3300 and 1160 ms^{-1}, respectively, with an uncertainty of about 10%. For all films, iterative determination of the domain size converged closely to the film thickness, indicating that only one crystallite is present along the entire thickness. An axially symmetric texture component is observed with an axis corresponding to the mean ⟨111⟩ direction aligned with the normal of the sample surface [Fig. 1(a)] as a regular columnar growth of fcc crystals. The orientation density background of around 0.6 m.r.d. [Fig. 1(a)] indicates that almost 60% of the crystallites are oriented differently from the main ⟨111⟩ texture component. Several samples were also prepared by rf sputtering technique for film deposition. The rf sputtered films exhibited a much larger maximum orientation density than dc sputtered films, i.e., 33 m.r.d. [Fig. 1(b)] vs 3 m.r.d. [Fig. 1(a)], respectively, emphasizing the broad orientation distribution in the latter films. Moreover, since there is no orientation density background for the rf sputtered films, no orientation other than ⟨111⟩ is present in significant amount.

The most relevant conclusions from the x-ray analysis are that on average the individual crystallites occupy the whole thickness of the films and that the orientations of 60% of the crystallites are different from the high symmetry texture ⟨111⟩ orientation. In other words, these dc gold sputtered structures can be seen as the transposition at the nanometric

a)Electronic mail: pezeril@mit.edu.

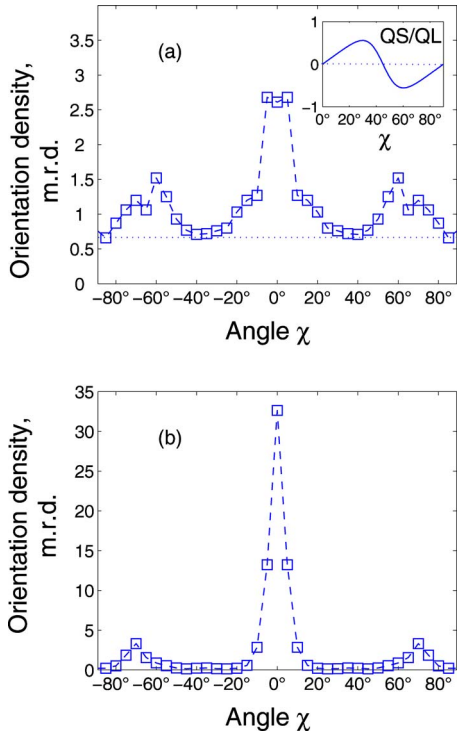

FIG. 1. (Color online) Radial distributions of the ⟨111⟩ crystallographic directions for two gold samples deposited by (a) dc sputtering and (b) rf sputtering. χ is the angle between the sample normal and the ⟨111⟩ crystallographic directions. The two lateral peaks at $\pm 70°$ reveal the multiplicity of the ⟨111⟩ directions for cubic symmetry. Orientation density units are in multiples of m.r.d. The simulated quasishear (QS) to quasilongitudinal (QL) photoacoustic amplitude ratio for different gold crystalline orientations is shown in the inset of (a).

scale of the results obtained earlier for a polycrystalline zinc sample,[4,7,22] and the theoretical arguments that justify shear generation and detection in both samples are similar. Simulations of photoacoustic wave generation[24] in gold single crystals show substantial quasishear amplitude for a broad range of orientations, to as much as ± 0.6 for $\chi = 30°, 60°$ [see Fig. 1(a) inset; $\chi = 0°$ when the ⟨111⟩ direction is collinear with the sample normal]. Thus many of the nanocrystallite orientations in the dc sputtered sample are expected to have significant shear generation efficiency. On the detection side, it is the deviation from isotropy in the photoelastic interaction that enables detection of the shear waves. Indeed, for any canted cubic medium, the change in dielectric coefficient $\delta\epsilon_S$ from shear strain η_S is proportional to $p_{44} - (p_{11} - p_{12})/2$.[22,23] Since $p_{44} \neq (p_{11} - p_{12})/2$ and χ is statistically nonzero in more than 60% of the film, the reflectometric detection of shear acoustic waves is qualitatively justified as well.[24]

For the picosecond photoacoustic experiments, we used a conventional pump-probe technique with a Ti:sapphire laser operating at 800 nm. The output is split into a pump and a variably delayed probe beam that are focused and crossed at the sample. Each pump pulse induces a thermal stress in the absorptive gold film that is responsible for photoacoustic excitation. The time-dependent probe reflectivity is sensitive to the acoustic perturbation of the dielectric coefficient $\delta\epsilon$, proportional to the strain. Results of reflectivity changes ΔR for the sample of thickness $H = 16.6$ nm are presented in Fig. 2. The two modes of vibration that we assume to be of mainly longitudinal (L) and shear (S) acoustic character are

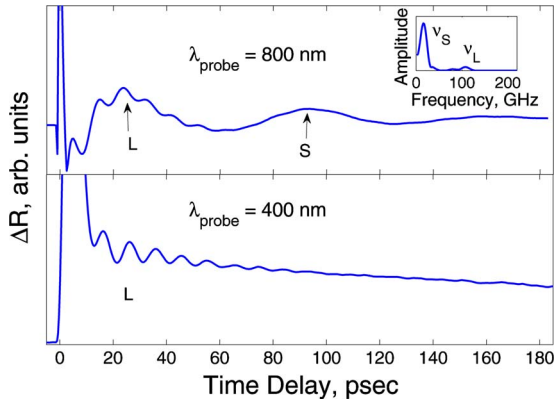

FIG. 2. (Color online) Picosecond dynamic reflectivity changes recorded for a gold film of thickness $H = 16.6$ nm. The laser pump wavelength is set to 800 nm, whereas the probe wavelength is either set to 800 or 400 nm. The Fourier transform of each reflectivity signal shown in the inset allows determination of the ringing frequencies ν_L and ν_S for each film thickness H.

clearly visible for an 800 nm probe wavelength. It is worth emphasizing that in gold films of ⟨111⟩ texture, as in the rf sputtered gold samples, no frequency except the longitudinal L frequency has been observed.[13] While probing with a probe wavelength of 400 nm instead of 800 nm, the shear wave is undetected in this case. This drastic difference suggests that the dispersion of the photoelastic coefficients p_{ij} with the probe wavelength results in a strong reduction at 400 nm in the magnitude of the combination $p_{44} - (p_{11} - p_{12})/2$ on which shear detection depends while the magnitude of the coefficient p_{12} that dictates the detection sensitivity for longitudinal strains is comparable at 400 and 800 nm probe wavelengths.

The longitudinal and shear resonance frequencies ν_L and ν_S, respectively, for all the film thicknesses have been extracted through Fourier analysis of the reflectivity signals and plotted versus $1/2H$ as shown in Fig. 3. The longitudinal frequencies follow the linear dispersion relation $\nu_L = c_L/2H$, where $c_L = 3340$ ms^{-1} is the mean longitudinal acoustic velocity deduced from the slope of the L mode of the dispersion curve of Fig. 3. This dispersion behavior is expected since the acoustic impedance $Z_L^{\mathrm{Au}}/Z_L^{\mathrm{Si}} \sim 3.3 > 1$. The shear mode frequencies follow the dispersion relation $\nu_S = c_S/4H$, where $c_S = 1040$ ms^{-1} is the mean shear acoustic velocity. This value is in close agreement with the expected shear speed of sound that corresponds to the broad maximum of the simulated quasishear photoacoustic excitation ($\chi = 30°$ and 60°). This dispersion behavior is expected if $Z_S^{\mathrm{Au}}/Z_S^{\mathrm{Si}} < 1$. The values that we determine for c_S and the gold film

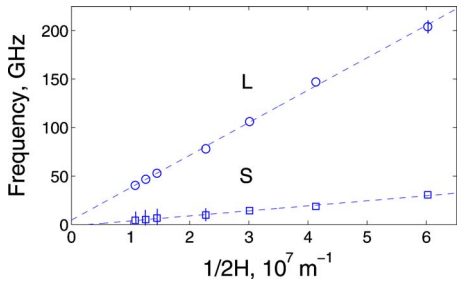

FIG. 3. (Color online) Dispersion curves of both longitudinal and shear modes from a set of seven gold films of different thicknesses H. The slopes give the average acoustic speeds in the films. The intercepts are zero within experimental uncertainties.

density (from the x-ray data) as well as the same parameters for Si would yield the opposite result, i.e., $Z_S^{\mathrm{Au}}/Z_S^{\mathrm{Si}} \sim 1.6 > 1$. We believe that this shear dispersion discrepancy could be a signature of poor adhesion of gold to silicon, as suggested by ultracentrifuge technique.[25] Alternatively, the low frequency response could represent the vibration of the entire film against the substrate,[12] with the frequency determined by the film thickness and the density as well as a force constant describing the van der Waals bonds[25] at the film-substrate interface. Such a model would yield a plausible value of the interface modulus. However, we do not see how the discrepancy between low-frequency and high-frequency signals from a modification of the probe wavelength can be rationalized in this model (see Fig. 2).

In summary, we have demonstrated an extension of picosecond shear wave generation and detection in gold films deposited on a silicon substrate through routine dc sputtering. The canted inhomogeneous nanostructure of the gold films, as revealed by x-ray reflectivity and diffraction, permit the generation and detection of picosecond quasishear waves. Innovative possibilities for generation and detection of ultrahigh-frequency shear waves are suggested by these results. The next step in this challenging problem will be the exploration of different deposition conditions and techniques and different materials to determine the extent of possible control over the asymmetric structure of the layers and the ranges of shear acoustic wave parameters that might be reached. We note that our results also suggest that thin film morphology may be assessed in some cases through picosecond photoacoustics.

This work was supported by CNRS and Région Basse-Normandie, and by the U.S. Army through the Institute for Soldier Nanotechnologies, under Contract No. DAAD-19-02-D-0002 with the U.S. Army Research Office. The authors are grateful to N. Chigarev and H. Leduc, LPEC, Le Mans, France, to C. Riter, IPTC, Berlin, Germany, and to C. Ecolivet, GMCM, Rennes, France.

[1] C. Thomsen, J. Strait, Z. Varcling, H. J. Maris, J. Tauc, and J. J. Hauser, Phys. Rev. Lett. **53**, 989 (1984).
[2] C. Thomsen, H. T. Grahn, H. J. Maris, and J. Tauc, Phys. Rev. B **34**, 4129 (1986).
[3] H. T. Grahn, H. J. Maris, and J. Tauc, IEEE J. Quantum Electron. **25**, 2562 (1989).
[4] T. Pezeril, P. Ruello, S. Gougeon, N. Chigarev, D. Mounier, J.-M. Breteau, P. Picart, and V. Gusev, Phys. Rev. B **75**, 174307 (2007).
[5] D. H. Hurley, O. B. Wright, O. Matsuda, V. E. Gusev, and O. V. Kolosov, Ultrasonics **38**, 470 (2000).
[6] O. Matsuda, O. B. Wright, D. H. Hurley, V. E. Gusev, and K. Shimizu, Phys. Rev. Lett. **93**, 095501 (2004).
[7] T. Pezeril, N. Chigarev, P. Ruello, S. Gougeon, D. Mounier, J.-M. Breteau, P. Picart, and V. Gusev, Phys. Rev. B **73**, 132301 (2006).
[8] T. Bienville and B. Perrin, Proceedings of WCU, 2003 (unpublished), p. 813 (sfa.asso.fr/wcu2003/procs/website/).
[9] G. Tas, R. J. Stoner, H. J. Maris, G. W. Rubloft, G. S. Oehrlein, and J. M. Halbout, Appl. Phys. Lett. **61**, 1787 (1992).
[10] B. Bonello, F. A. Armand, J.-P. Pradeau, H. Perez, B. Perrin, and G. Louis, J. Appl. Phys. **86**, 4959 (1999).
[11] B. Bonello, G. Louis, and P. Battioni, Rev. Sci. Instrum. **74**, 889 (2003).
[12] G. Tas, J. J. Loomis, H. J. Maris, A. A. Bailes, and L. E. Seiberling, Appl. Phys. Lett. **72**, 2235 (1998).
[13] G. A. Antonelli, B. Perrin, B. C. Daly, and D. G. Cahill, MRS Bull. **31**, 607 (2006).
[14] H.-N. Lin, R. J. Stoner, H. J. Maris, J. M. E. Harper, C. Cabral, J.-M. Halbout, and G. W. Rubloff, Appl. Phys. Lett. **61**, 2700 (1992).
[15] J. Daillant and A. Gibaud, *X-ray and Neutron Reflectivity* (Springer, New York, 1999), pp. 87–115.
[16] D. Chateigner (www.ecole.ensicaen.fr/~chateign/texture/combined.pdf).
[17] H.-J. Bunge and C. Esling, in *Quantitative Texture Analysis*, edited by H.-J. Bunge and C. Esling (DGM, Oberursel, Germany, 1982).
[18] D. Chateigner, J. Appl. Crystallogr. **38**, 603 (2005).
[19] S. Matthies and G. W. Vinel, Phys. Status Solidi B **112**, 111 (1982).
[20] H.-R. Wenk, S. Matthies, J. Donovan, and D. Chateigner, J. Appl. Crystallogr. **31**, 262 (1998).
[21] S. Matthies and M. Humbert, J. Appl. Crystallogr. **28**, 254 (1995).
[22] T. Pezeril, Ph.D. thesis, Université du Maine, 2005 (http://tel.archives-ouvertes.fr/tel-00011291/fr/).
[23] B. A. Auld, *Acoustic Fields and Waves in Solids*, 2nd ed. (Krieger, Malabar, FL, 1990), Vol. 1, p. 80.
[24] T. Pezeril, V. Gusev, D. Mounier, N. Chigarev, and P. Ruello, J. Phys. D **38**, 1421 (2005).
[25] G. Bohme, P. Hohn, H. Krupp, H. Rabenhorst, W. Schnabel, and G. Walter, J. Appl. Phys. **44**, 3914 (1973).